Low-force spectroscopy on graphene membranes by scanning tunneling microscopy

Supplementary Material

B. Uder*[1], H. Gao[1], P. Kunnas[2], N. de Jonge[2] and U. Hartmann[1]

[1]*Institute of Experimental Physics, Saarland University, Saarbruecken, D-66041, Germany*
[2]*INM- Leibnitz Institute for New Materials, Saarbruecken, D-66123, Germany*

*bernd.uder@uni-saarland.de

SEM Imaging

The sample was studied by scanning electron microscopy (ThermoFischer, Quanta 250 ESEM). Imaging under an angle of 75°(Fig. S1) reveals graphene-covered and empty holes with sharp edges at the rim of the holes. The radius of the holes was measured by averaging the areas of 29 holes and amounted to $a = (1.21 \pm 0.02)$µm. The contrast

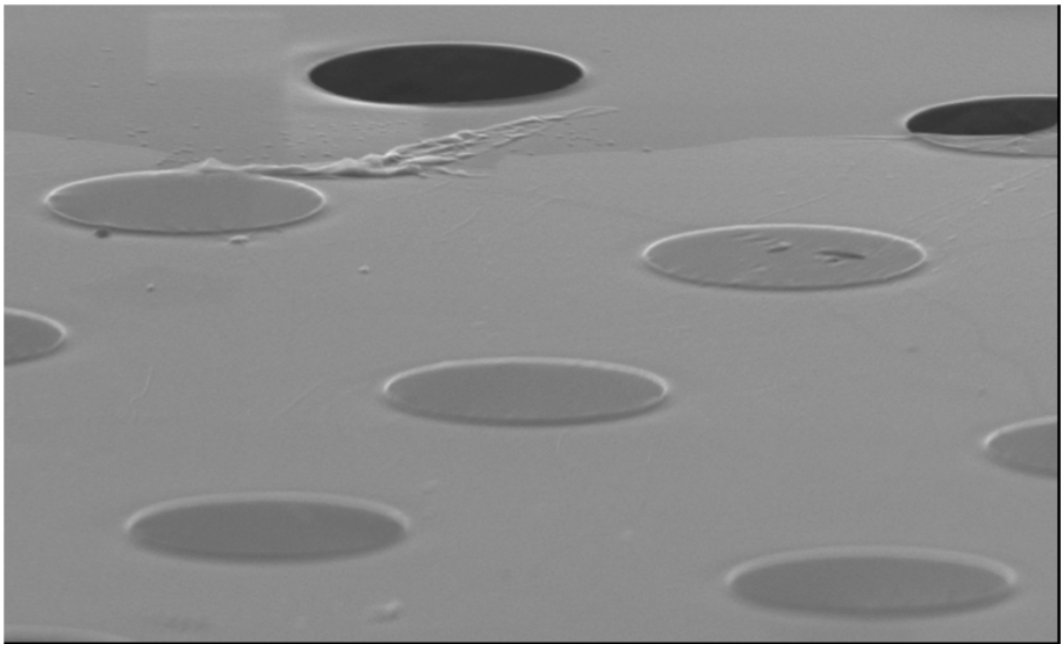

Figure S1: SEM imaging of a graphene-covered and empty holes. The magnification is 30,000x, the electron beam energy is 5 keV, and the specimen was tilted by an angle of 75°.

is dominated by secondary electrons. For a given penetration depth of the primary electrons, more secondary electrons result from the supported areas in comparison to the freestanding graphene membrane [1]. This causes a higher signal from the substrate and the sharp edge in contrast. The sharp edge is clearly visible in the intensity line-profile (Fig. S2). The line profile in Figure S2(b)) implies a deep pit of the membrane inside the hole. However, this is only due to the lower yield of secondary electrons and does not reveal topography information.

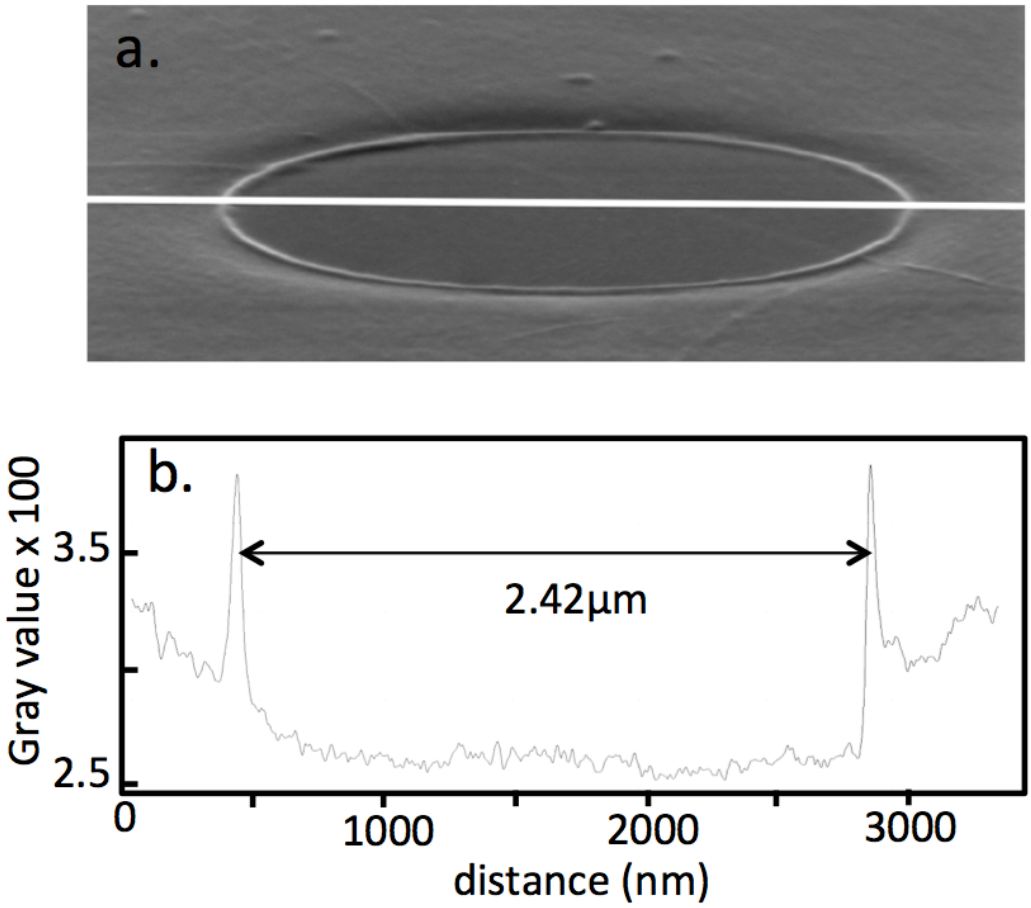

Figure S2: (a) SEM imaging of a graphene-covered hole. The magnification is 120,000x, the electron beam energy is 5 keV, and the specimen was tilted by an angle of 75°. (b) Line-profile.

AFM imaging

AFM imaging of the sample reveals a diameter of $(2.8 \pm 0.2)\mu m$ (Fig. S3) due to the convolution of tip and hole geometry. Details of the membrane profile reveal a steep

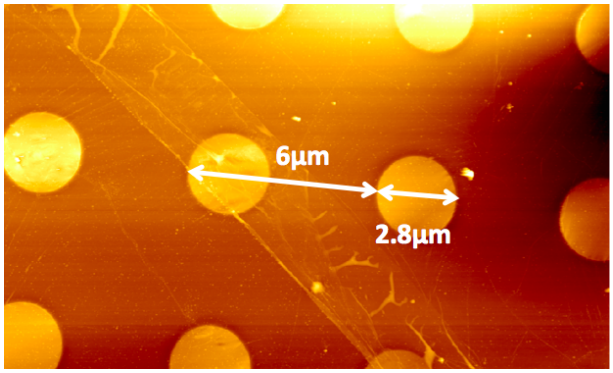

Figure S3: AFM images of the graphene covered grid.

rise at the edge within (100±20)nm, a height of approximately 30nm (Fig. S4) and a smooth curve across the membrane.

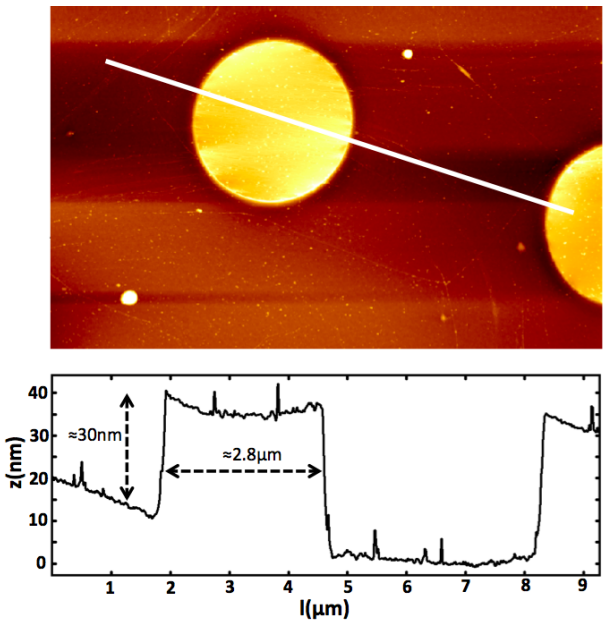

Figure S4: AFM images of a membrane with line profile (unprocessed raw data).

STM line-profile scans

Membrane line-profile scans were recorded across a graphene membrane at varying sample bias (V) from +0.1V to +2.5V (Fig. S5). V increments after each line by +0.1V. The image representation of all lines recorded is shown in Figure S5a revealing a sharp transition at the membrane edge for all voltages and with constant membrane diameter. This proofs that the tip pulling on the membrane is not detaching the membrane from the substrate within the applied force range. The small lateral shift seen is due to a constant thermal drift at room temperature.

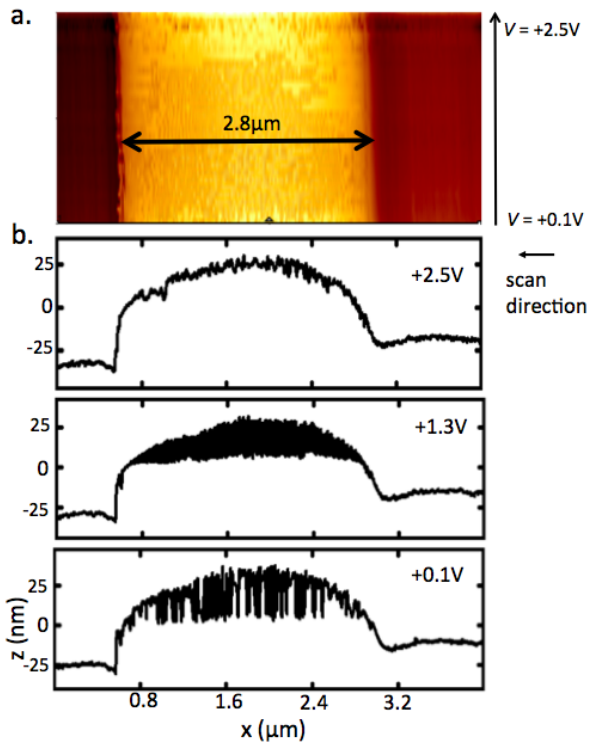

Figure S5: STM line-profile scans: I=100pA, loop gain 2%, 40s/line, 2000 data points in x direction, 20ms/data point. (a) Image of profile scans recorded from +0.1V to +2.5. The voltage increment is 0.1V after each line. (b) Selected line profiles for +0.1V, +1.3V, +2.5V.

The tunneling distance

The tunneling distance between the tip and the surface was measured using a quasi-static method. The tunneling current I and the vertical tip position z were monitored simultaneously over time during STM with active feedback on highly oriented pyrolytic graphite (HOPG). I_t was toggled between different values. Correlating $z(t)$ with $I(t)$ data reveals the mutual relation between I and z. The data for the relative distance change Δz are shown in Figure S6. The interpolation gives a tunneling distance of $z_0 = (1.2 \pm 0.1)$nm for a sample bias of V = -50mV at a tunneling current at I =10pA. The advantage of this method compared to the standard $I(z)$-spectroscopy with open feedback loop is that it is for low tunneling currents close to the noise limit.

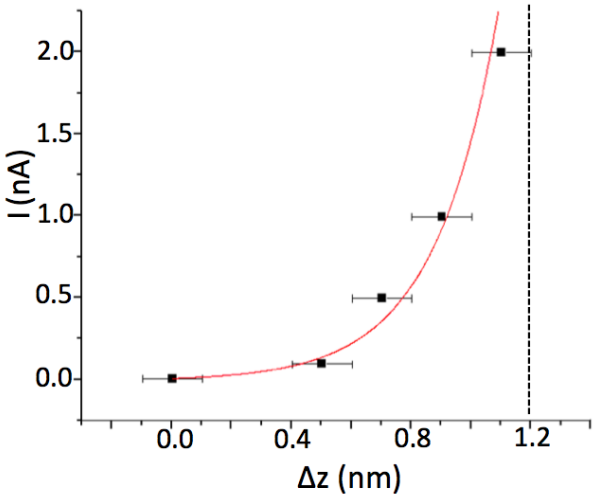

Figure S6: Relative distance change $\Delta z = z(10\,\text{pA})$ - $z(I)$ with active feedback and $V = -50\,\text{mV}$ on HOPG.

Details of a spectroscopy curve

A comparison of data for release and pull directions for the *flip-down* and *flip-up* regions (Fig. 3 of the main article) is shown in Figure S7. For the release direction a correlation of z and I clearly manifests a loss of the tunneling contact before the flip down occurs.

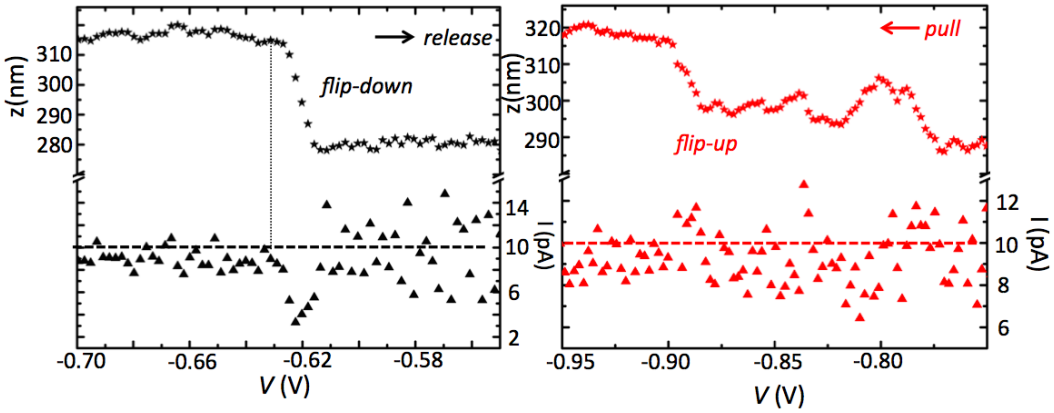

Figure S7: Zoom of flip-down (black) and flip-up (red) region. Time per data point is 100ms.

The pull direction reveals a cascade-like transition in the flip-up regime. Correlating z and I data reveals an interplay between the tunneling current error signal and the integral distance controller[2] with iterative tip-retract and approach cycles until a stable position is reached.

Force calibration

Approximating the geometry of the tip in tunneling contact by a sphere of radius r at a close distance z_0 to a plane surface yields a relation between the applied voltage V and the electrostatic force [3]. The electrostatic force F_{el} is given by

$$F_{el} = -\frac{\pi\epsilon_0 V^2 r}{z_0(1+ln(V/V_0))} \quad . \tag{1}$$

Equation 1 was used for the force calibration of the data of Fig. 2(e) of the main article. Figure S8 shows raw data together with the curve $F_{el}(V)$ (black) with the parameters used for the force calibration of $z(V)$-data. The accuracy of the force calibration is affected by the accuracy of the determination of the tip radius r and the tunneling distance z_0:

$$\Delta F_{el} = \left|\frac{\delta F_{el}}{\delta r}\right| \Delta r + \left|\frac{\delta F_{el}}{\delta z_0}\right| \Delta z_0 \quad , \tag{2}$$

$$\Delta F_{el} = \left|-\frac{\pi\epsilon_0 V^2}{z_0(1+ln(V/V_0))}\right| \Delta r + \left|\frac{\pi\epsilon_0 V^2 r}{z_0^2(1+ln(V/V_0))}\right| \Delta z_0 \quad . \tag{3}$$

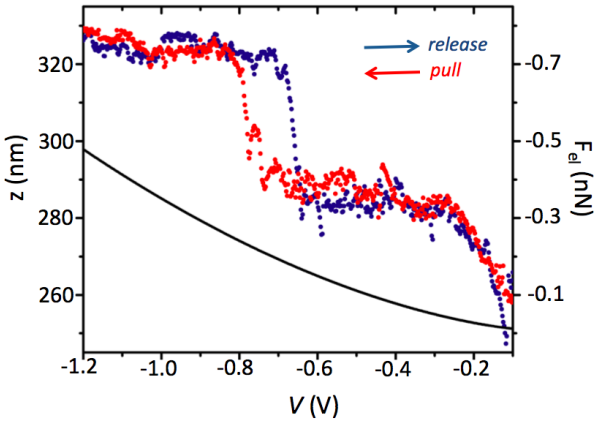

Figure S8: Raw data of measurement shown in Fig. 2e of the main article together with the force calibration curve for the parameters z_0=1.2 nm, r=50nm, V_0=−0.1 V.

SEM imaging (Fig. S9) reveals a tip radius of $r = (50 \pm 10)$nm. The tunneling distance is $z_0 = (1.2 \pm 0.1)$nm at $V = 0.1$ V. ΔF_{el} increases with V^2 but this is balanced by the

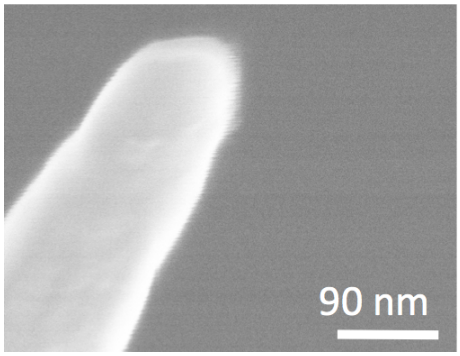

Figure S9: SEM images (Hitachi S-800) of the used tungsten tip.The magnification was 300,000x, the electron beam energy was 30 keV,

increase of the tunneling distance with increasing voltage. The error for the maximum force used in the experiment at V = -1.2V, r = 50nm and with z_0 = 1.2nm is

$$\Delta F_{el}(-1.2V) = 10 \cdot 10^{-12} \frac{N}{m} \cdot \Delta r + 400 \cdot 10^{-12} \frac{N}{m} \cdot \Delta z_0 \ . \tag{4}$$

With the estimated error Δr = 10nm and Δz_0 = 0.1nm one obtains:

$$\Delta F_{el}(-1.2V) = 100pN + 40pN \ . \tag{5}$$

This yields a total error of F_{el} of approximately 30%. The result in equation 5 shows that the estimation of the tip radius is important for the accuracy of the force calibration. An overview for selected V values is shown in table S1.

V (V)	F_{el} (nN)	ΔF_{el} (nN)	error (%)
-0.6	-0.15	0.04	27
-0.8	-0.24	0.07	29
-1.2	-0.48	0.14	29

Table S1: Accuracy of the force calibration for selected V.

The in-plane elastic modulus

Applying the bulge-test equations, the in-plane elastic modulus (E_{2D}) amounts to [4, 5]

$$E_{2D} = (1-\nu)\frac{3a^2 F_{el}}{8\pi(\Delta h_4)^3} \quad . \tag{6}$$

The Poisson number ν increases with system size up to 0.275 [6]. This is then applied for the micrometer-sized membrane. A force of $F_{el} = (0.48 \pm 0.14)$nN deflects the membrane by $\Delta h_4 = (h_4 - h_3) = (6.5 \pm 0.5)$nm. The membrane radius is $a = (1210 \pm 20)$nm. Inserting this into equation 6 gives $E_{2D} = 220$N/m for the strained membrane in region IV (see Figure 4 of main article).
The accuracy of E_{2D} is determined by the error ΔF_{el} of the force calibration, Δa of the membrane radius and Δh_4^{error} of the height change in region IV. The total error ΔE_{2D} is

$$\Delta E_{2D} = \left|\frac{\delta E_{2D}}{\delta a}\right| \Delta a + \left|\frac{\delta E_{2D}}{\delta F_{el}}\right| \Delta F_{el} + \left|\frac{\delta E_{2D}}{\delta \Delta h_4}\right| \Delta h_4^{error} \quad ,$$

which results in

$$\Delta E_{2D} = (1-\nu)\left(\left|\frac{6aF_{el}}{8\pi\Delta h_4^3}\right| \Delta a + \left|\frac{3a^2}{8\pi\Delta h_4^3}\right| \Delta F_{el} + \left|\frac{9a^2 F_{el}}{8\pi\Delta h_4^4}\right| \Delta h_4^{error}\right) \quad .$$

Applying this to the experimental data one obtains

$$\Delta E_{2D} = (1-\nu)\,(10 + 89 + 70)\,N/m \approx 120 N/m \quad .$$

The elastic modulus measured is thus $E_{2D} = (220 \pm 120)$N/m.

The radial in-plain strain

The in-plane strain ϵ_r is given by [4, 5]

$$\epsilon_r = \frac{2(h_3 - h_1)^2}{3a^2} \quad .$$

The experimental data yields $h_3 - h_1 = (48 \pm 5)$nm corresponding to an in-plane strain of $\epsilon_r = (0.10 \pm 0.02)\%$.

Membrane fluctuations

Local measurements of $z(t)$ at the membrane center show aperiodic low-frequency fluctuations (marked by the green line) at low voltages with amplitudes between 1 and 2nm(Figure S10). The distance regulation is fast enough to follow these slow variations in z as indicated by the tunneling current I which is very stable at the set point of 9pA with deviations in the order of less than 3pA. High-frequency contributions are seen in the tunneling current (red curve) which likely results from external sources and which are above the regulation bandwidth of 1kHz used in the experiment.

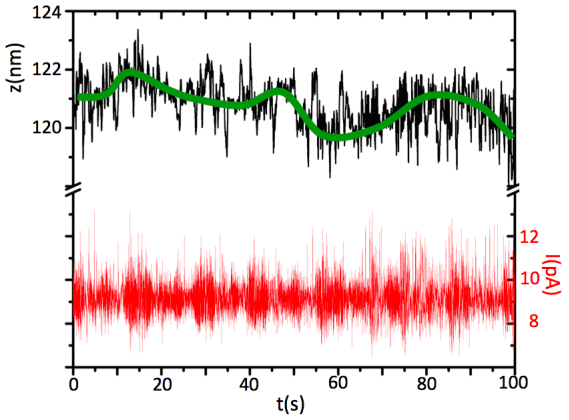

Figure S10: Measurement at membrane center: $z(t)$ (black), $I(t)$ (red). V = -10mV, I = 9pA. The measurement shows 10000 data points at a raster time of 10ms with a sampling rate of 400kHz.

The real-time oscilloscope monitor (Fig. S11) shows this aperiodic motion of z in real time.

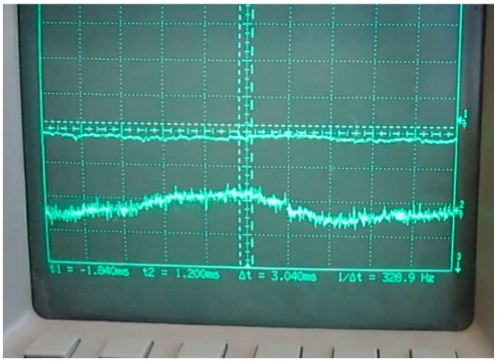

Figure S11: Screen shot of a realtime oscilloscope image. I (upper curve), z (lower curve). Trigger: 10ms unit.

References

[1] J.C. Bouwer, T.J. Deerinck, E. Bushong, V. Astakhov, R. Ramachandra, S.T. Peltier, and M.H Ellisman. *Deceleration of probe beam by stage bias potential improves resolution of serial block-face scanning electron microscopic images*. Adv. Struct. Chem. Imag. **2**, 11 (2016).

[2] B. Uder and U. Hartmann. *A convenient method for large-scale STM mapping of freestanding atomically thin conductive membranes*. Rev. Sci. Instr. **88**, 063702 (2017).

[3] Franz J. Giessibl. *Advances in atomic force microscopy*. Rev. Mod. Phys. **75**, 949 (2003).

[4] M.K. Small and W.D. Nix. *Analysis of the accuracy of the bulge test determing the mechanical properties of thin films*. J. Mater. Res. **7**, 1553 (1992).

[5] R.J.T. Nicholl, H.J. Conley, N.V. Lavrik, I. Vlassiouk, Y.S. Puzyrev, V.P. Sreenivas, S.T. Pantelides and K.I. Bolotin. *The effect of intrinsic crumpling on the mechanics of free-standing graphene*. Nat. Comm. **6**, 9789 (2015).

[6] J.H. Los, A. Fasolino, and M.I. Katsnelson. *Scaling Behavior and Strain Dependence of In-Plane Elastic Properties of Graphene*. Phys. Rev. Lett. **116**, 015901 (2016).